ACS APPLIED MATERIALS & INTERFACES

Research Article

www.acsami.org

Effects of Ga:N Addition on the Electrical Performance of Zinc Tin Oxide Thin Film Transistor by Solution-Processing

Byung Du Ahn,[†,∥] Hye Ji Jeon,[‡,∥] and Jin-Seong Park*[,‡]

[†]School of Electrical and Electronic Engineering, Yonsei University, 50 Yonsei-ro, Seodaemun-gu, Seoul 120-749, Korea

[‡]Division of Materials Science and Engineering, Hanyang University, 222 Wangsimni-ro, Seoul, 133-719, Republic of Korea

ABSTRACT: This paper addressed the effect of gallium nitrate hydrate addition on thin film transistor (TFT) performance and positive bias stability of amorphous zinc tin oxide (ZTO) TFTs by solution processing, Further, the mechanisms responsible for chemical properties and electronic band structure are explored. A broad exothermic peak accompanied by weight loss appeared in the range from about 350 to 570 °C for the ZTO solution; the thermal reaction of the Ga-ZTO:N solution was completed at 520 °C. This is because the gallium nitrate hydrate precursor promoted the decomposition and dehydroxylation reaction for $Zn(CH_3COO)_2{\cdot}2H_2O$ and/or $SnCl_2{\cdot}2H_2O$ precursors. The concentrations of carbon and chloride in gallium nitrate hydrate added ZTO films annealed at 400 °C have a lower value (C 0.65, Cl 0.65 at. %) compared with those of ZTO films (C 3.15, Cl 0.82 at. %). Absorption bands at 416, 1550, and 1350 cm^{-1} for GaZTO:N films indicated the presence of $ZnGa_2O_4$, N−H, and N═O groups by Fourier transform infrared spectroscopy measurement, respectively. As a result, an inverted staggered Ga-ZTO:N TFT exhibited a mobility of 4.84 $cm^2\ V^{-1}\ s^{-1}$ in the saturation region, a subthreshold swing of 0.35 V/decade, and a threshold gate voltage (V_{th}) of 0.04 V. In addition, the instability of V_{th} values of the ZTO TFTs under positive bias stress conditions was suppressed by adding Ga and N from 13.6 to 3.17 V, which caused a reduction in the oxygen-related defects located near the conduction band.

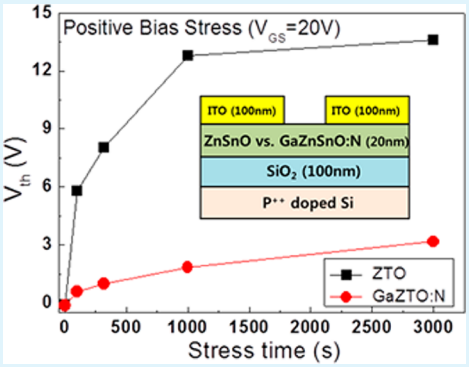

KEYWORDS: *oxide semiconductor thin film transistor, nitrogen doping, solution process, zinc tin oxide*

1. INTRODUCTION

Oxide semiconductor (OS) thin film transistors (TFTs) are promising candidates that can be incorporated in a variety of electronic applications, including large-area display panels such as liquid crystal displays (LCDs) and organic light-emitting diodes (OLEDs).[1,2] The major attractive aspects are their high mobility, excellent uniformity, low processing temperature, and high transparency. Generally, a vacuum-based deposition process, i.e., radio frequency magnetron sputtering, has been used for the preparation of oxide channel layers because it allows facile control over carrier concentrations by adjusting operating conditions. However, this technique has the disadvantage of a high manufacturing cost. During recent decades, solution-processed OS have been intensively investigated for realizing low-cost processed electronics (e.g., printing technique) for flexible displays and/or flat panel active matrix displays by continuous-solution processes.[3,4] A simple process, high throughput, and low cost are advantages of solution-processed OSs.[5−7] Nevertheless, a solution-processed oxide semiconductor still suffers from lower performance; further, a higher-temperature annealing process than the vacuum-based method is required in order to obtain high-quality OSs. For achieving high-performance TFTs, numerous methods have also been proposed, including development of novel oxide semiconductor materials using combinatorial material designs using solution processes.[8] For example, the TFTs using solution-processed oxide semiconductors, such as InZnO (IZO), InGaZnO (IGZO), and InZnSnO (IZTO), have been already studied intensively.[9−11]

Although an indium and gallium element in the active channel layer are essential for assuring excellent channel mobility and stability, respectively, their scarcity of resources and high price are critical issues to apply in mass-produced electronics. Thus, ZnSnO (ZTO) has been recently attractive as a promising active layer due to its low cost and elemental abundance.[12]

Previous studies have reported that the precursors and annealing temperature conditions play important roles to improve electrical properties of the solution-based ZTO TFTs.[13,14] Jeong et al.[15] reported the electrical property of ZTO TFTs using tin acetate $[Sn(CH_3COO)_2]$ and zinc acetate dehydrate $[Zn(CH_3COO)_2{\cdot}2H_2O]$ as the Sn and Zn precursors, respectively. The TFT performance exhibited a field-effect mobility (μ_{FE}) of 1.1 $cm^2/(V{\cdot}s)$ when the channel layer was annealed at a high-temperature of 500 °C. Kim et al.[13] reported the device properties under various annealing temperatures, including the photobias instability of ZTO TFTs fabricated using $ZnCl_2$ and $SnCl_2$ precursors. Up to

Received: March 7, 2014
Accepted: June 3, 2014
Published: June 3, 2014

600 °C, the annealing process showed a significant improvement of device performance in the ZTO TFTs. Unfortunately, they used high-temperature annealing methods (up to 500 °C) to obtain high performance of ZTO TFTs, which are not compatible with a realization of practical metal-oxide electronics.

Recently, two studies reported the effect of gallium doping on IZO TFT performance solution-processed in order to reduce the process temperature. Jeong et al.[6] studied solution-based amorphous Ga-doped IZO films and found out the alternative role of Ga lowering the temperature of film processing. Banger et al.[9] also reported that Ga doping is a route for forming high-performance IZO TFTs at low process temperatures under 250 °C. However, there is still a lack of both an understanding of the effect of gallium doping on device performances of solution-processed ZTO TFTs and information to support the variations in electrical and chemical properties.

In vacuum-based deposited OS TFTs, nitrogen doping has an effect on TFT performance and stability. Raja et al.[16] reported the effect of nitrogen doping on amorphous InGaZnO thin-film transistors regarding the device performance and stability. Nitrogen doping can passivate defects and/or dangling bonds in InGaZnO films, which reduced oxygen vacancies and charge-trap density. Huang et al.[17] addressed an ultrathin interfacial InGaZnO:N layer to improve the bias stress stability on a-InGaZnO TFTs. As already mentioned above, the formation of Ga−N bonds can suppress the concentration of oxygen vacancies within the layer. Unfortunately, there has been a lack of information available with regard to nitrogen doping in solution-processed ZTO TFTs. Therefore, a more detailed analysis based on chemical and electrical behavior is necessary to investigate the mechanism governing overall TFT performance and stability of Ga added ZTO:N TFTs as an oxide channel layer.

2. EXPERIMENTAL SECTION

Precursor Solution Preparation. The ZTO and GaZTO solutions were prepared for dissolving tin chloride dihydrate [$SnCl_2 \cdot 2H_2O$, 98% (Aldrich)], zinc acetate dehydrate [$Zn(CH_3COO)_2 \cdot 2H_2O$, 98% (Aldrich)], and gallium nitrate hydrate [$Ga(NO_3)_3 \cdot H_2O$, 99.9%] in 2-methoxyethanol [$CH_3OCH_2CH_2OH$, 98% (Aldrich)], with a concentration of 0.2 M. The molar ratios of ZTO and GaZTO precursor solutions were 50:50 (Zn:Sn) and 5:47.5:47.5 (Ga:Zn:Sn), respectively. 2-Methoxyethanol is well-known to be a versatile solvent due to good solubility and low viscosity, also acting as a stabilizer.[18] These clear solutions were stirred using a magnetic bar for 6 h at 60 °C before spin-coating.

Film Deposition. Each precursor solution was stirred and filtered by using the previous sequence.[14] After preparing the solution, spin-coating was carried out at a spin speed of 3000 rpm for 30 s. Then, the coated layer was dried at 150 °C on a hot plate for 15 min. After that, the heating process was done at 400 °C directly for 1 h in air. The spin-coated films had a thickness of about 20 nm, as measured by spectroscopic ellipsometry (SE).

TFT Fabrication. Heavily doped silicon (p-type) substrates with 100 nm thick SiO_2 were used as the gate and insulator. The substrates were treated by oxygen plasma for 1 min at a power of 10 W to enhance the coating properties before coating the active layer.

After the films (ZTO and GaZTO) were deposited on the treated insulator layer, indium tin oxide with a thickness of 100 nm was deposited as the source and drain electrodes (the channel length: 200 μm and the channel width: 800 μm). The indium tin oxide was formed by radio frequency sputtering through a shadow mask.

Characterization. Thermal properties of the samples were examined by thermal gravimetric analysis and differential thermal analyses (TGA−DTA; model SDT Q600, Auto-DSCQ20 system). The crystallinity of the films (ZTO and GaZTO) was measured by X-ray diffraction (XRD, D/MAX-2500/PC). The chemical structure of the films was determined by Fourier transform infrared spectroscopy (FT-IR, WQF-510A, Shenyang Faith Trading Co.) and X-ray photoelectron spectroscopy (XPS, Theta Probe, Thermo Fisher Scientific Co). Auger electron spectroscopy (AES, PHI 680) was used to obtain elemental compositions of films. The spectroscopy ellipsometry (SE) was used with an auto retarder in the energy range of 0.75−6.4 eV with incident angles of 65, 70, and 75°. The characteristics of the TFTs were evaluated with an HP 4145B in a dark room at ambient conditions.

3. RESULTS AND DISCUSSION

Figure 1 shows the thermogravimetric and differential thermal analyses (TG−DTA) curves of ZTO, GaZTO, and GaO_x precursor solutions measured under a dry air atmosphere with a heating rate of 3 °C/min up to 600 °C. As shown in

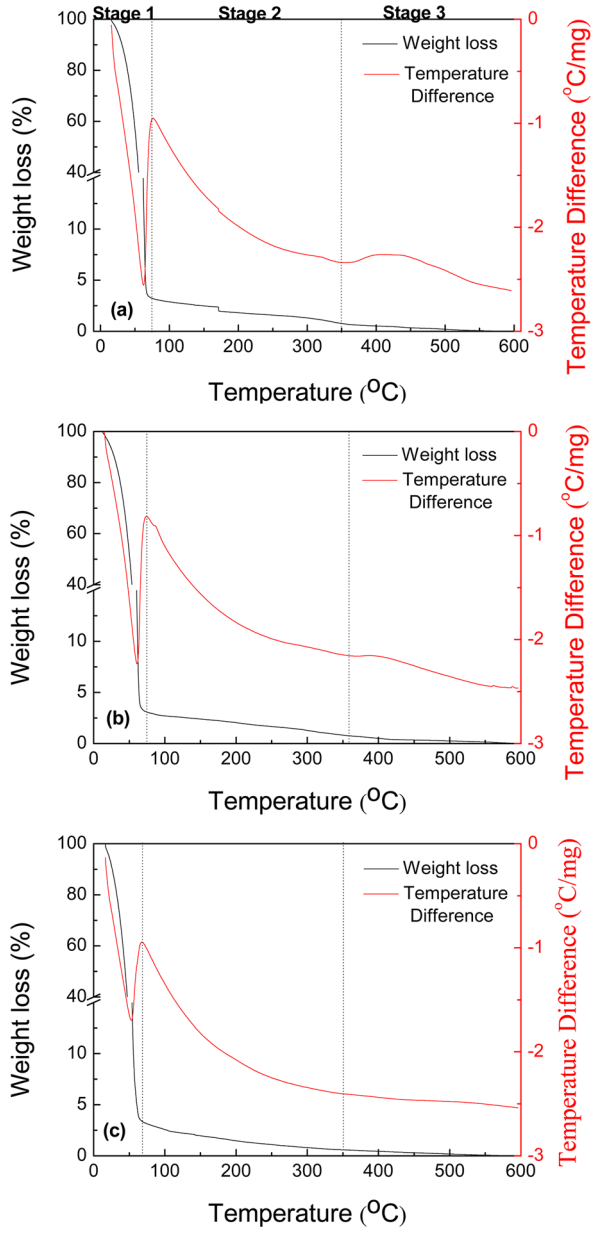

Figure 1. TGA and DSC curves of (a) ZTO, (b) GaZTO, and (c) GaO_x solution under air (heating speed: 3 °C/min).

dx.doi.org/10.1021/am5013672 | ACS Appl. Mater. Interfaces 2014, 6, 9228−9235

Figure 1, there are three stages based on all the solutions by TG−DSC analyses: decomposition and hydrolysis, dehydroxylation and alloy, and densification. The initial main weight loss (~90%) of all the solutions happened in the range of 25−90 °C; during this stage, an endothermic reaction with a peak at about 60 °C was observed in the heat flow analysis. This phenomenon happened in all solutions independent of precursor. This is due to the thermal reaction related to the decomposition and hydrolyzation of the precursor. In the three different solutions, $Zn(CH_3COO)_2{\cdot}2H_2O$, $SnCl_2{\cdot}2H_2O$, and $Ga(NO_3)_3{\cdot}H_2O$ were decomposed and then hydrolyzed to $Zn(OH)_2$, $SnCl_2$, and $Ga(OH)_2NO_3$.[14,19] The evaporation of the H_2O, 2-methoxyethanol, CH_3COOH, and HNO_3 contributed to the initial weight loss. In stage 2, the exothermic reactions were observed to be accompanied with a small weight loss in the temperature range of 90−350 °C. This phenomenon can be explained by three kinds of formation mechanisms depending on the precursor. For $Zn(OH)_2$, dehydroxylation occurred. $SnCl_2$ underwent the sol−gel process, which should eliminate organic residues after hydrolysis and condensation reactions. $Ga(OH)_2NO_3$ gradually lost N_2O_5 and, though the formation of unstable oxy-nitrate, was transformed into gallium oxide.[19] In stage 3, the broad exothermic peak accompanied by a very small weight loss appeared in the range from 350 to 570 °C for the ZTO solution and from 350 to 520 °C for the Ga-ZTO:N solution, respectively, which can be an alloy reaction of M−OH. Futher, the small weight loss was due to the residual material decomposition after stage 2.

To verify whether phase transformation occurs during annealing, we analyzed high-resolution X-ray diffraction patterns of ZTO and GaZTO thin films annealed at temperatures of 400 °C, shown in Figure 2. The X-ray

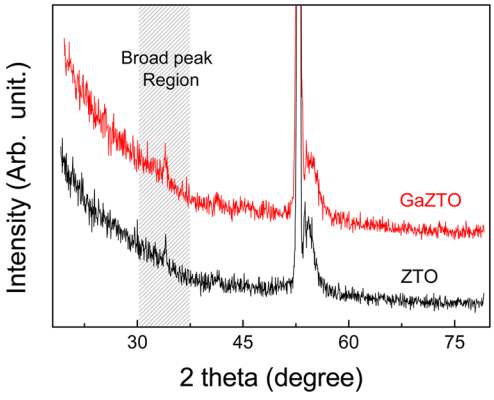

Figure 2. XRD results of the ZTO and GaZTO thin films annealed at 400 °C.

diffraction profiles exhibited an amorphous-like broad peak located at around 34°, and sharp crystalline peaks were observed at 51.5° and 54.5°. Strong crystalline peaks at 51.5° and 54.5° originated from the substrate of SiO_2 (thickness) 100 nm/Si (100).[15] Recently, two studies were reported about the structure of the ZTO film depending on annealing temperature. Jeong et al.[15] reported that the ZTO films (zinc acetate dehydrate ($Zn(CH_3COO)_2{\cdot}2H_2O$) and tin acetate ($Sn(CH_3COO)_2$)) annealed at 500 °C were composed of amorphous materials in which approximately 1−2 nm sized particles were embedded. Kim et al.[13] also reported a locally crystallized volume portion of 30−40% in the amorphous matrix at 600 °C (ZTO). They used a $ZnCl_2$ and $SnCl_2$ precursor to synthesize ZTO films. This peak at around 34°corresponded with a Zn_2SnO_4 (311) peak (JCPDS 73-1725) or a GaZnO (or ZnO) peak (JCPDS 48-0484). Peak positions were very similar, so it was difficult to determine the main peak position in this result. Kovacheva et al.[20] reported that trigonal-ilmenite $ZnSnO_3$ and cubic-spinel Zn_2SnO_4 are formed at relativley low temperatures (<600 °C) and high temperatures (>1000 °C), respectively. Thus, the broad peak at around 34° was attributed to the (002) peak of ZnO or GaZnO, which is the amorphous phase that has a locally crystallized structure reported previously.[21] With Ga precursor addition, the position of an amorphous-like broad peak was shifted from 34° to 33.8°. This was thought to result from Ga−Zn−O texturing because Ga can substitute in Zn sites, thus reducing the number of defects; this is possible because the radius of the Ga ion (Ga−O (1.92 Å)) is similar to that of the Zn ion (Zn−O (1.97 Å)).[22]

To confirm the residual material after thermal reaction at 400 °C annealing, a locally crystallized phase was detected by XRD analysis. FT-IR absorption spectra for ZTO and Ga-ZTO films between 400 and 4000 cm^{-1} are shown in Figure 3a. All the

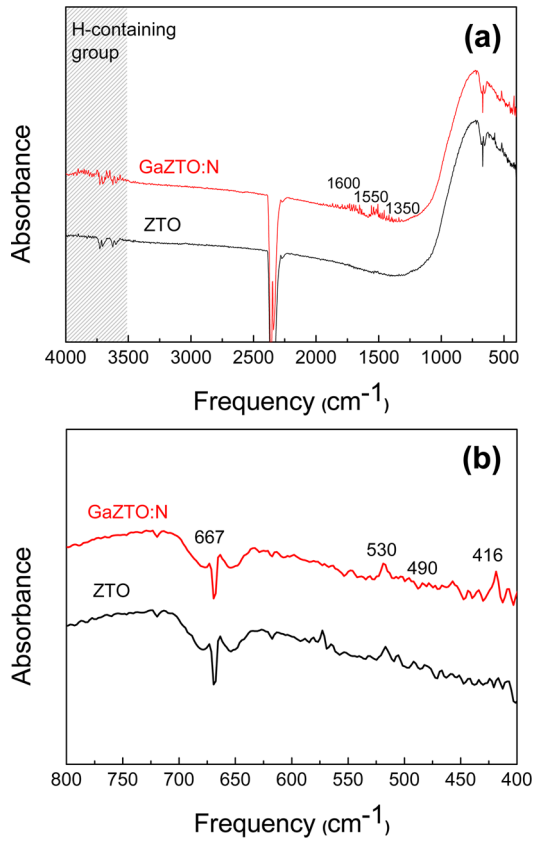

Figure 3. FT-IR spectroscopy of the ZTO and GaZTO:N films over (a) 4000−400 cm^{-1} and (b) 800−400 cm^{-1}.

spectra were similar in the range of 400−4000 cm^{-1}. The bands located at 3500−4000 cm^{-1} are attributed to the hydroxyl free −OH group of the solvent adsorbed on the surface of films.[23] The bands located around 1600 cm^{-1} corresponded to the stretching mode of the C−N. Further, the band centered at 1550 and 1350 cm^{-1} corresponds to the bending mode of N−H and N═O groups.[24−26] As shown in FT-IR analysis, nitrogen would be attributed to the bonding of unstable oxy-nitrate from the $Ga(NO_3)_3{\cdot}H_2O$ precursor. In the 800−400 cm^{-1} spectral range, as shown in Figure 3b, ZTO and GaZTO

dx.doi.org/10.1021/am5013672 | ACS Appl. Mater. Interfaces 2014, 6, 9228−9235

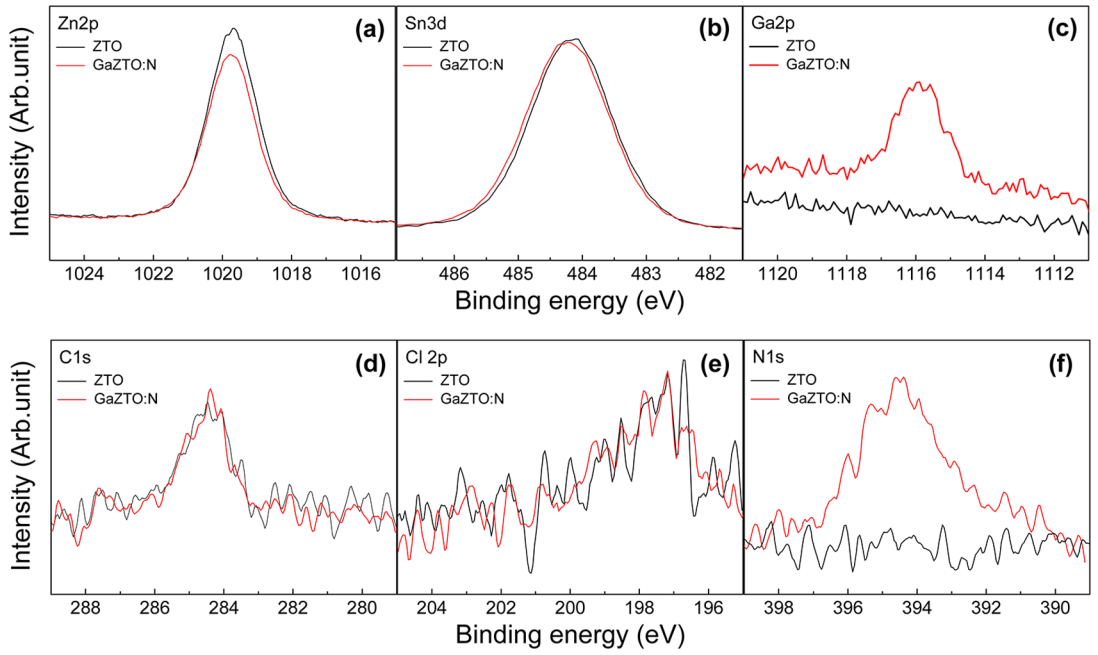

Figure 4. XPS spectra of the (a) Zn 2p, (b) Sn 3d, (c) Ga 2p, (d) C 1s, (e) Cl 2p, and (f) N 1s core-level line for ZTO and GaZTO:N films.

samples revealed several peaks. Thus, Ga-ZTO films can be denoted as GaZTO:N by FT-IR analysis. For the ZTO and Ga-ZTO:N initial mixture, the typical absorption band of the SnO_2 lattice was at 667 cm^{-1} and those of the Zn−O bond around 530−490 cm^{-1} were noticed. However, relevant changes in the FT-IR spectrum of the Ga-ZTO film can be seen by the appearance of new absorption bands at 416 cm^{-1} assigned to $ZnGa_2O_4$, which was consistent with results obtained by XRD measurements.

With various Zn/Sn ratios and residue material from the precursor, ZTO films exhibited different device performances.[15] To quantitatively analyze cation composition and residue such as carbon, chloride, and nitrogen even after thermal annealing in both the ZTO and GaZTO:N films, XPS analysis was performed. Figure 4a−f shows the XPS spectra of the Zn 2p, Sn 3d, Ga 2p, C 1s, Cl 2p, and N 1s core levels, respectively. The binding energy (BE) of the Ga $2p_{3/2}$ level from Ga_2O_3 typically showed at 1116.7 eV, and that of the Zn $2p_{3/2}$ level from ZnO showed at 1022 eV. The BE of the Sn $3d_{3/2}$ level was present around 485 eV, which can be assigned to SnO. The BEs of C 1s, Cl 2p, and N 1s are shown at 284.5, 197.1, and 394.5 eV, respectively.[27] From the XPS results, the atomic percentages of Zn, Sn, Ga, C, Cl, and O atoms were derived and are shown in Table 1. The few chlorine atoms originated from the $SnCl_2$ precursor. The BE of N 1s overlapped that of the Auger peak of Ga 2p by XPS using an Al source. To avoid this argument, the N concentration was measured for the ZTO and Ga-ZTO:N films by AES. As a result, the N concentration of the GaZTO:N films was 1.6 at. %, wherein the N atoms in GaZTO:N originated from unstable oxy-nitrate from the $Ga(NO_3)_3{\cdot}H_2O$ precursor.

Table 1. Summary of Elemental Compositions in ZTO and GaZTO:N Films (at. %)

	Zn	Sn	Ga	O	C	Cl	N
ZTO	25.92	26.76	0	3.15	3.15	0.82	0
GaZTO:N	21.58	23.53	6.68	2.89	0.65	0.65	2.08

Figure 5 exhibits the transfer characteristics of ZTO and GaZTO:N annealed at 400 °C. The μ_{FE} in the saturation region

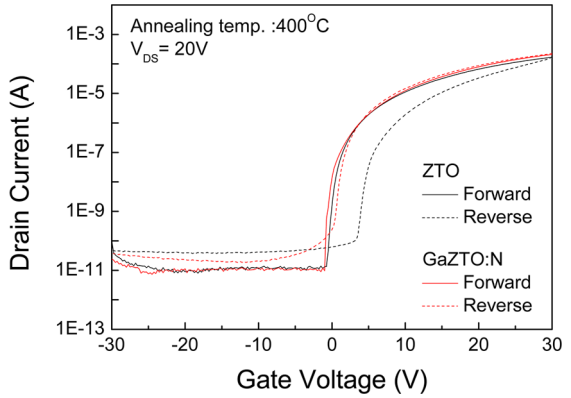

Figure 5. Representative transfer curves of ZTO and GaZTO:N TFTs under forward and reverse bias.

(drain-to-source voltage, V_{DS} = 20 V) and subthreshold swing (SS) values were extracted, according to the expression for a field-effect transistor.[28] The extracted device parameters are summarized in Table 2. The ZTO device exhibited a μ_{FE}, SS value, and V_{th} of 3.61 $cm^2/(V{\cdot}s)$, 0.45 V/decade, and −0.09 V, respectively. On the other hand, improved performance was observed in the GaZTO:N device with a μ_{FE}, SS value, and V_{th} of 4.84 $cm^2/(V{\cdot}s)$, 0.35 V/decade, and 0.04 V, respectively. The SS value is generally related to the total trap density of a given TFT device, including the semiconductor−insulator interfacial traps (D_{it}) and bulk (N_{SS}), by the following equation[29]

$$SS = \frac{qk_BT(N_{SS}t_{ch} + D_{it})}{C_i \log(e)}$$

where q, k_B, T, and t_{ch} are the electron charge, Boltzmann's constant, the absolute temperature, and channel layer thickness,

dx.doi.org/10.1021/am5013672 | ACS Appl. Mater. Interfaces 2014, 6, 9228−9235

Table 2. Electrical Characteristics of the ZTO and GaZTO:N Channel Layers Annealed at 400°C in Air for 1 h

				N_{total}	
	V_{th} (V)	mobility ($cm^2/(V{\cdot}s)$)	SS (V/decade)	N_{SS} (10^{18}/eV cm^3)	D_{it} (10^{12}/eV cm^2)
ZTO	−0.09	3.61	0.45	0.88	1.59
GaZTO:N	0.04	4.84	0.35	0.68	1.24

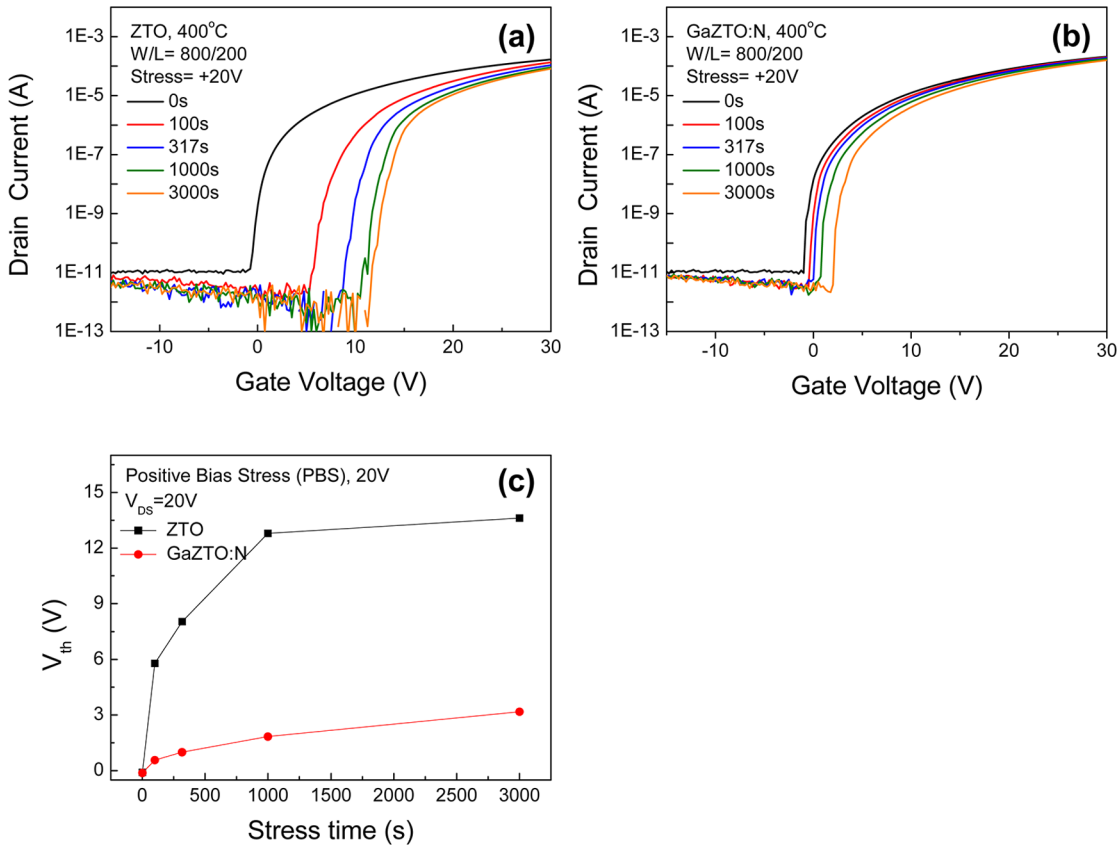

Figure 6. Transfer characteristics of (a) ZTO and (b) GaZTO:N TFTs with positive threshold voltage shift and (c) threshold voltage shift (ΔV_{th}) as a function of stress time.

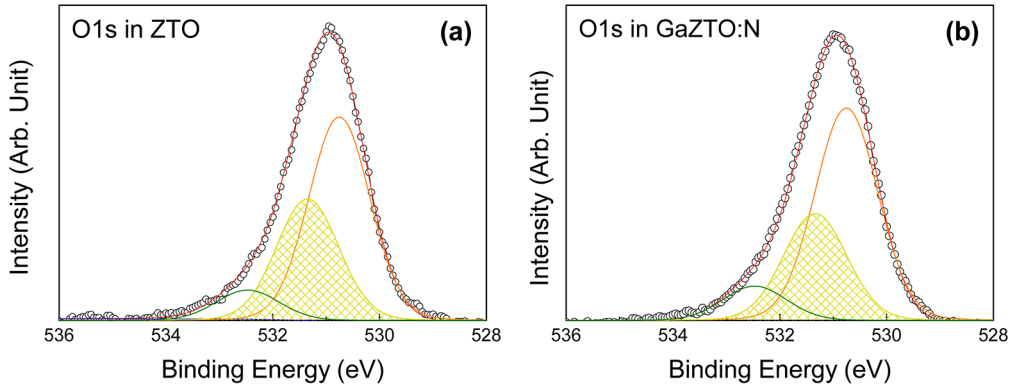

Figure 7. XPS spectra of the O 1s core-level line for the (a) ZTO and (b) GaZTO:N films.

respectively. The calculated N_{SS} and D_{it} values are also included in Table 1. For example, the N_{SS} and D_{it} values for the ZTO device were 8.8×10^{17} eV^{-1} cm^{-3} and 1.59×10^{12} eV^{-1} cm^{-2}, respectively, and these values decreased to 6.8×10^{17} eV^{-1} cm^{-3} and 1.24×10^{12} eV^{-1} cm^{-2}, respectively, for a GaZTO:N device. Therefore, the improvement in TFT performance for GaZTO:N devices can be attributed to the reduced N_{SS} and/or D_{it} because electron charge trapping is linearly increased with the total number of available trap sites at the GaZTO:N interface and/or bulk region.[29] This suggests that the charge-trapping defects are reduced by the addition of Ga precursor. In addition, the transfer curve in a reverse V_{GS} sweep from 30 to −30 V was positively displaced compared to that in a forward V_{GS} sweep from −30 to 30 V. The hysteresis of Ga-ZTO:N TFTs is described by the red dotted line, whereas the black dotted line in Figure 5 shows the larger hysteresis of the ZTO

dx.doi.org/10.1021/am5013672 | ACS Appl. Mater. Interfaces 2014, 6, 9228−9235

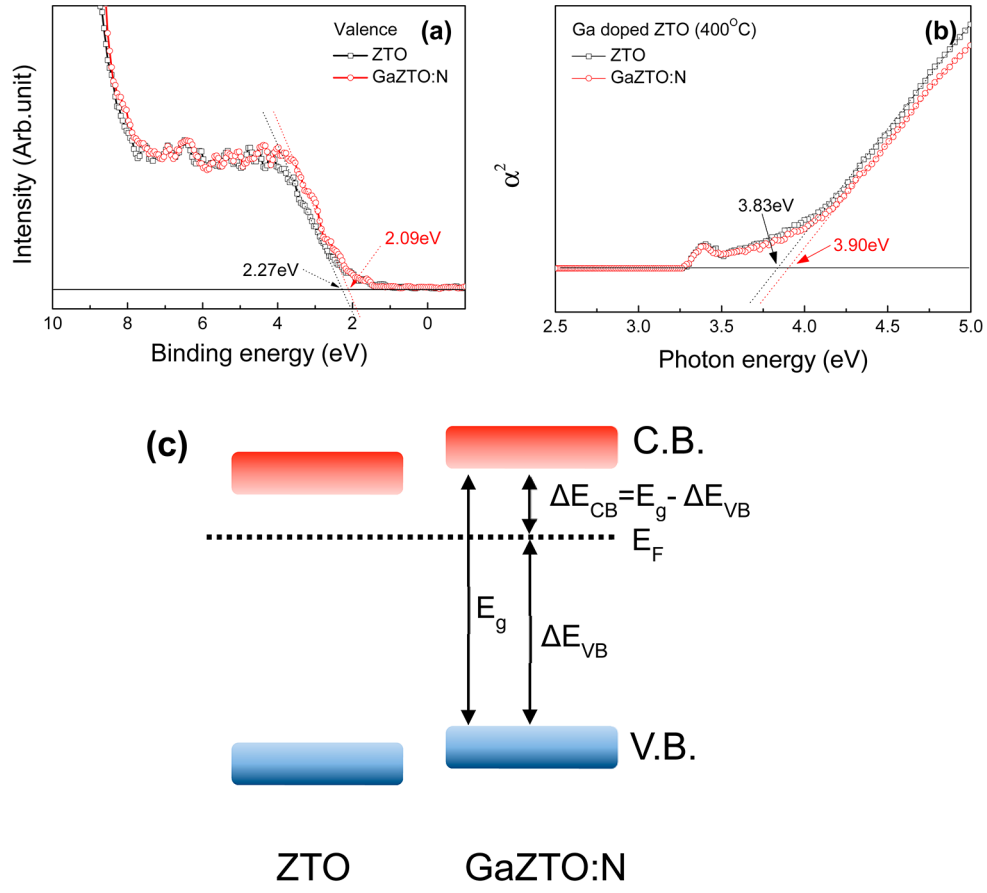

	Eg(eV)	ΔE_{VB}(eV)	ΔE_{CB}(eV)
ZTO	3.83	2.27	1.56
GaZTO:N	3.90	2.09	1.81

Figure 8. (a) Near valence band edge peak (XPS spectra), (b) optical band gap (SE measurement), and (c) schematic band-alignment energy diagram indicating the relative energy position of the E_F (Fermi level), CBM (conduction band minimum), and VBM (valence band maximum).

TFT. However, there was no significant hysteresis in GaZTO:N TFTs. Thus, the enhanced mobility of GaZTO:N TFTs would originate from decreasing charge trap densities due to the addition of Ga element.

The effects of Ga precursor addition in ZTO on the positive bias stress (PBS) instability were investigated in Figure 6. The TFTs were stressed by the following conditions: Applying with V_{GS} = −20 V and V_{DS} = 20 V at room temperature for 3000 s. As the stress time passed by, the V_{th} values of ZTO and GaZTO:N TFTs systematically increased to the positive direction, without any meaningful changes of μ_{FE} and SS values. For the ZTO device, a large positive V_{th} shift of 13.6 V with increasing PBS time was observed (see Figure 6a). Interestingly, the device for the GaZTO:N exhibited a significantly smaller V_{th} shift of 3.17 V under identical PBS conditions.

To understand the origin of the above improvements, we may mainly consider the chemical bonding states and electronic structure (the Fermi-level band alignment). First, XPS was measured to find out the changes in chemical bonding states on the ZTO films due to addition of Ga precursor. Figure 7a,b displays the O 1s spectra for the ZTO and GaZTO:N films. Before collecting XPS spectra of both films, the Ne ions sputtering (at 500 eV) was treated on the films to remove the surface contamination such as OH, C, H_2O, etc. The O 1s peaks were split by using a Gaussian profile, which exhibited an intense peak at around 530.7 ± 0.1 eV along with a broad shoulder peak at 531.3 ± 0.2 and 532.4 ± 0.2 eV. The O 1s peaks at 530.7, 531.3, and 532.4 eV are correlated with metal−oxygen bonding states (no oxygen deficiency), oxygen deficient states of the ZTO system, and the hydroxyl groups on the surfaces, respectively.[30] It is noted that the relative area of the oxygen vacancy-related peak decreased from 34% (ZTO) to 30% (GaZTO:N). This implies that Ga precursor addition is more effective to reduce the oxygen deficiencies than ZTO, which can be attributed to suppression of oxygen vacancy generation in GaZTO films.[21] In addition, N doping in GaZTO films controls the trap density by suppressing defect-related

dx.doi.org/10.1021/am5013672 | ACS Appl. Mater. Interfaces 2014, 6, 9228−9235

oxygen vacancies, as in the case of a-IGZO:N films.[16] Therefore, the GaZTO:N films have much smaller oxygen-related defects such as oxygen-deficient bonding states, which can explain the superior transport properties of the resulting TFTs.

In order to understand the subgab states below the conduction band, the absorption coefficient spectra were extracted through SE analysis on the ZTO and GaZTO:N films. In Figure 8a,b, it is clearly shown that the absorption via subgap states below the band gap (E_g) was considerably reduced by addition of Ga precursor. Taking the ZTO films as a reference, the relative ratio of subgap states decreased from 1.27 (ZTO films) to 1 (GaZTO:N), which can be attributed to the decrease in oxygen vacancy concentration.

Next, using the extrapolation method, the valence band spectra and E_g were extracted by XPS and SE, respectively, and the schematic energy band diagram for ZTO and GaZTO:N films[31] is shown in Figure 8c. The corresponding values of E_g and the relative energy difference between the Fermi level (E_F) and valence band maximum (ΔE_{VB}), and between E_F and the conduction band minimum (ΔE_{CB}), are indicated below the diagram. The extracted E_g increased from 3.83 eV (ZTO) to 3.90 eV (GaZTO:N), while the valence band offset (ΔE_{VB}) decreased from 2.27 eV (ZTO) to 2.09 eV (GaZTO:N). As a result, the relative position of the Fermi level (ΔE_{CB}) moved from 1.56 eV (ZTO) to 1.81 eV (GaZTO:N). This can result in a decrease of carrier concentration in the GaZTO:N semiconductor. Generally, it has been reported that higher carrier concentration may lead to higher mobility in oxide TFTs due to the percolation theory.[32] However, considering the enhancement of device performances (GaZTO), it may originate from the suppression and passivation of oxygen-related defects due to the addition of Ga and N. The addition of Ga and N in ZTO may play important roles to improve mobility and bias stability, although the ΔE_{CB} is larger in the GaZTO semiconductor.

4. CONCLUSION

In summary, this study examined the effect of gallium nitrate hydrate addition on the thermal reaction, chemical properties, TFT performance, and positive bias instability of ZTO TFTs. Gallium nitrate hydrate added ZTO films annealed at 400 °C have lower chloride and carbon concentrations compare to those of ZTO films. On the other hand, N atoms originating from unstable oxy-nitrate from gallium nitrate hydrate served as additional dopants in addition to Ga atoms. For these reasons, it was demonstrated that GaZTO:N exhibited significantly improved PBS-induced instability compared to those of ZTO TFTs. This is due to the strong oxidation power of Ga atoms and consequent effective reduction of oxygen-related defects, which act as electron traps and are located at subgap states within the band gap. Therefore, the enhanced stability against PBS for GaZTO:N was attributed to the reduction in V_O defect density in the ZTO film, which strongly supports the instability mechanism involving charge trapping related to oxygen defects. We suggest that the combined approach of Ga and N would be a promising method for high-performance and highly stable ZTO TFT fabrication in next-generation displays

AUTHOR INFORMATION

Corresponding Author

*E-mail: jsparklime@hanyang.ac.kr.

Author Contributions

[‖]These two authors contributed equally to this work.

Notes

The authors declare no competing financial interest.

ACKNOWLEDGMENTS

This research was supported by the Global Frontier Program through the Global Frontier Hybrid Interface Materials (GFHIM) of the National Research Foundation of Korea (NRF) funded by the Ministry of Science, ICT & Future Planning (2013M3A6B1078870) and partially done by the IT R&D program of MKE/KEIT (Grant No. 10041416. The core technology development of light and space adaptable new mode display for energy saving on 7 in. and 2 W).

REFERENCES

(1) Nomura, K.; Ohta, H.; Takagi, A.; Kamiya, T.; Hirano, M.; Hosono, H. Room-Temperature Fabrication of Transparent Flexible Thin-Film Transistors Using Amorphous Oxide Semiconductors. *Nature* **2004**, *432*, 488−492.

(2) Park, J. S.; Kim, H.; Kim, D. I. Overview of Electroceramic Materials for Oxide Semiconductor Thin Film Transistors. *J. Electroceram.* **2013**, DOI: 10.1007/s10832-013-9858-0.

(3) Sun, Y.; Rogers, J. A. Inorganic Semiconductors for Flexible Electronics. *Adv. Mater.* **2007**, *19*, 1897−1916.

(4) Ju, S. H.; Facchetti, A.; Xuan, Y.; Liu, J.; Ishikawa, F.; Ye, P.; Zhou, C. W.; Marks, T. J.; Janes, D. B. Fabrication of Fully Transparent Nanowire Transistors for Transparent and Flexible Electronics. *Nat. Nanotechnol.* **2007**, *2*, 378−384.

(5) Song, K.; Noh, J.; Jun, T.; Jung, T.; Jung, Y.; Kang, H. Y.; Moon, J. Fully Flexible Solution-Deposited ZnO Thin-Film Transistors. *Adv. Mater.* **2010**, *22*, 4308−4312.

(6) Jeong, S.; Ha, Y. G.; Moon, J.; Facchetti, A.; Marks, T. J. Role of Gallium Doping in Dramatically Lowering Amorphous-Oxide Processing Temperatures for Solution-Derived Indium Zinc Oxide Thin-Film Transistors. *Adv. Mater.* **2010**, *22*, 1346−1350.

(7) Adamopoulos, G.; Bashir, A.; Thomas, S.; Gillin, W. P.; Georgakopoulos, S.; Shkunov, M.; Baklar, M. A.; Stingelin, N.; Maher, R. C.; Cohen, L. F.; Bradley, D. D. C.; Anthopoulos, T. D. Spray-Deposited Li-Doped ZnO Transistors with Electron Mobility Exceeding 50 cm^2/Vs. *Adv. Mater.* **2010**, *22*, 4764−4769.

(8) Kim, M. G.; Kanatzidis, M.; Facchetti, A.; Marks, T. J. Low-Temperature Fabrication of High-Performance Metal Oxide Thin-Film Electronics via Combustion Processing. *Nat. Mater.* **2011**, *10*, 382−388.

(9) Banger, K. K.; Yamashita, Y.; Mori, K.; Peterson, R. L.; Leedham, T.; Rickard, J.; Sirringhaus, H. Low-Temperature, High-Performance Solution-Processed Metal Oxide Thin-Film Transistors Formed by a 'Sol−gel on Chip' Process. *Nat. Mater.* **2010**, *10*, 45−50.

(10) Koo, C. Y.; Song, K.; Jun, T.; Kim, D.; Jeong, Y.; Kim, S. H.; Ha, J.; Moon, J. Low Temperature Solution-Processed InZnO Thin-Film Transistors. *J. Electrochem. Soc.* **2010**, *157*, J111−J115.

(11) Kim, M. G.; Kim, H. S.; Ha, Y. G.; He, J.; Kanatzidis, M. G.; Facchetti, A.; Marks, T. J. High-Performance Solution-Processed Amorphous Zinc-Indium-Tin Oxide Thin-Film Transistors. *J. Am. Chem. Soc.* **2010**, *132*, 10352−10364.

(12) Tsaroucha, M.; Aksu, Y.; Irran, E.; Driess, M. Synthesis of Stannyl-Substituted Zn_4O_4 Cubanes as Single-Source Precursors for Amorphous Tin-Doped ZnO and Zn_2SnO_4 Nanocrystals and Their Potential for Thin Film Field Effect Transistor Applications. *Chem. Mater.* **2011**, *23*, 2428−2438.

(13) Kim, Y. J.; Yang, B. S.; Oh, S.; Han, S. J.; Lee, H. W.; Heo, J.; Jeong, J. K.; Kim, H. J. Photobias Instability of High Performance Solution Processed Amorphous Zinc Tin Oxide Transistors. *ACS Appl. Mater. Interfaces* **2013**, *5*, 3255−3261.

(14) Zhao, Y.; Dong, G.; Duan, L.; Qiao, J.; Zhang, D.; Wang, L.; Qiu, Y. Impacts of Sn Precursors on Solution-Processed Amorphous

Zinc−Tin Oxide Films and Their Transistors. *RSC Adv.* **2012**, *2*, 5307−5313.
(15) Jeong, S.; Jeong, Y.; Moon, J. Solution-Processed Zinc Tin Oxide Semiconductor for Thin-Film Transistors. *J. Phys. Chem. C* **2008**, *112*, 11082−11085.
(16) Raja, J.; Jang, K.; Balaji, N.; Choi, W.; Trinh, T. T.; Yi, J. Negative Gate-Bias Temperature Stability of N-doped InGaZnO Active-Layer Thin-Film Transistors. *Appl. Phys. Lett.* **2013**, *102*, 083505.
(17) Huang, X.; Wu, C.; Lu, H.; Ren, F.; Chen, D.; Zhang, R.; Zheng, Y. Enhanced Bias Stress Stability of a-InGaZnO Thin Film Transistors by Inserting an Ultra-Thin Interfacial InGaZnO:N layer. *Appl. Phys. Lett.* **2013**, *102*, 193505.
(18) Schwartz, R. W. Chemical Solution Deposition of Perovskite Thin Films. *Chem. Mater.* **1997**, *9*, 2325−2340.
(19) Berbenni, V.; Milanese, C.; Bruni, G.; Marini, A. Thermal Decomposition Of Gallium Nitrate Hydrate $Ga(NO_3)_3$ xH_2O. *J. Therm. Anal. Calorim.* **2005**, *82*, 401−407.
(20) Kovacheva, D.; Petrov, K. Preparation of crystalline $ZnSnO_3$ from Li_2SnO_3 by Low-Temperature Ion Exchange. *Solid State Ionics* **1998**, *109*, 327−332.
(21) Jeong, Y. M.; Bae, C. D.; Kim, D. J.; Song, K. K.; Woo, K. H.; Shin, H. J.; Cao, G.; Moon, J. H. Bias-Stress-Stable Solution-Processed Oxide Thin Film Transistors. *ACS Appl. Mater. Interfaces* **2010**, *2*, 611−615.
(22) Cong, G. W.; Wei, H. Y.; Zhang, P. H.; Peng, W. Q.; Wu, J. J.; Liu, X. L.; Jiao, C. M.; Hu, W. G.; Zhu, Q. S.; Wang, Z. G. One-Step Growth of ZnO from Film to Vertically Well-Aligned Nanorods and the Morphology-Dependent Raman Scattering. *Appl. Phys. Lett.* **2005**, *87*, 231903.
(23) Griffiths, D. M.; Rochester, C. H. Infrared Study of the Adsorption of Water onto the Surface of Rutile. *J. Chem. Soc., Faraday Trans. 1* **1997**, *73*, 1510.
(24) Pekel, N.; Sahiner, N.; Akkas, P.; Güven, O. Uranyl Ion Adsorptivity of N-Vinyl 2-pyrrolidone/Acrylonitrile Copolymeric Hydrogels Containing Amidoxime Groups. *Polym. Bull.* **2000**, *44*, 593−600.
(25) Chang, M. C.; Tanaka, J. FT-IR Study for Hydroxyapatite/Collagen Nanocomposite Cross-Linked by Glutaraldehyde. *Biomaterials* **2002**, *24*, 4811−4818.
(26) Sundaraganesan, N.; Ilakiamani, S.; Sallen, H.; Wojciechowski, P. M.; Michalska, D. FT-Raman and FT-IR Spectra, Vibrational Assignments and Density Functional Studies of 5-Bromo-2-nitropyridine. *Spectrochim. Acta, Part A* **2005**, *6*, 2995−3001.
(27) Moulder, J. F.; Stickle, W. F.; Sobol, P. E.; Bomben, K. D. In *Handbook of X-ray Photoelectron Spectroscopy: A Reference Book of Standard Spectra for Identification and Interpretation of XPS Data*; Chastain, J., King, R. C., Eds.; Physical Electronics: Eden Prairie, MN, 1995; pp 40−62.
(28) Park, J. S.; Jeong, J. K.; Mo, Y. G.; Kim, H. D.; Kim, C. J. Control of Threshold Voltage in ZnO-Based Oxide Thin Film Transistors. *Appl. Phys. Lett.* **2008**, *93*, 033513.
(29) Park, S. Y.; Ji, K. H.; Jung, H. Y.; Kim, J. I.; choi, R.; Son, K. S.; Ryu, M. K.; Lee, S.; Jeong, J. K. Improvement in the Device Performance of Tin-Doped Indium Oxide Transistor by Oxygen High Pressure Annealing at 150 °C. *Appl. Phys. Lett.* **2012**, *100*, 162108.
(30) Kim, Y. H.; Heo, J. S.; Kim, T. H.; Park, S.; Yoon, M. H.; Kim, J.; Oh, M. S.; Yi, G. R.; Noh, Y. Y.; Park, S. K. Flexible Metal-Oxide Devices Made by Room Temperature Photochemical Activation of Sol−Gel Films. *Nature* **2012**, *489*, 128−133.
(31) Park, H. W.; Kim, B. K.; Park, J. S.; Chung, K. B. Device Performance and Bias Instability of Ta Doped InZnO Thin Film Transistor as a Function of Process Pressure. *Appl. Phys. Lett.* **2013**, *102*, 102102.
(32) Ahn, B. D.; Lim, J. H.; Cho, M.-H.; Park, J. S.; Chung, K. B. Thin-Film Transistor Behaviour and the Associated Physical Origin of Water-Annealed In−Ga−Zn Oxide Semiconductor. *J. Phys. D: Appl. Phys.* **2012**, *45*, 415307.